Published in final edited form as:
Nat Methods. 2011 March ; 8(3): 242–245. doi:10.1038/nmeth.1569.

High-throughput single-molecule optofluidic analysis

Soohong Kim[1,8], **Aaron M Streets**[2,8], **Ron R Lin**[1], **Stephen R Quake**[2,3,4], **Shimon Weiss**[1,5,6], and **Devdoot S Majumdar**[1,7]

[1]Department of Chemistry and Biochemistry, University of California, Los Angeles, Los Angeles, California, USA.

[2]Department of Applied Physics, Stanford University, Stanford, California, USA.

[3]Department of Bioengineering, Stanford University, Stanford, California, USA.

[4]Howard Hughes Medical Institute, Stanford, California, USA.

[5]Department of Physiology, University of California, Los Angeles, Los Angeles, California, USA.

[6]California NanoSystems Institute, University of California, Los Angeles, Los Angeles, California, USA.

Abstract

We describe a high-throughput, automated single-molecule measurement system, equipped with microfluidics. the microfluidic mixing device has integrated valves and pumps to accurately accomplish titration of biomolecules with picoliter resolution. We demonstrate that the approach enabled rapid sampling of biomolecule conformational landscape and of enzymatic activity, in the form of transcription by *Escherichia coli* RNA polymerase, as a function of the chemical environment.

Biological function is context-dependent, and *in vitro* study of a biological system is often limited to a predefined chemical environment chosen to recapitulate facets of the system's function *in vivo*[1]. As a result, *in vitro* studies may overlook real biological phenomena by undersampling the many chemical environments available in the cell. Here we describe a new method that can be used to easily screen many hundreds of chemical environments to aid in the construction of a ‘phase diagram’ of biological function in the context of chemical space.

A widely adopted readout of biomolecule conformation (or interaction) is single-molecule fluorescence resonance energy transfer (smFRET), wherein a single donor-acceptor pair reports on the distance between dyes on the 1–10 nm scale[2], a technique used to study an ever-growing list of macromolecules (helicases, polymerases and ribosomes, to name a few). Microfluidic technology enables precise and rapid handling of small liquid volumes

Correspondence should be addressed to D.S.M. (devdoot@caltech.edu) or S.W. (sweiss@chem.ucla.edu)..
[7]Present address: Division of Biology, California Institute of Technology, Pasadena, California, USA.
[8]These authors contributed equally to this work.

author contributions

S.K., A.M.S. and D.S.M. designed experiments, conducted experiments, wrote and implemented data acquisition and analysis software, and analyzed data. R.R.L. analyzed data. S.K., A.M.S., S.R.Q., S.W. and D.S.M. assisted in writing and editing of the manuscript.

Note: Supplementary information is available on the Nature Methods website.

COMPETING FINANCIAL INTERESTS

The authors declare no competing financial interests.

and thus facilitates large-scale screening of biological molecules with minimal sample consumption3›4. The integration of optics and microfluidics is rapidly becoming a useful tool in single-molecule biophysics: microfluidic systems are used for hydrodynamic focusing in single-molecule studies of protein folding5¯8, as 'gradient generators' in large-scale ensemble FRET measurements[9] and gas-controlled smFRET measurements[10], and as formulators[11] capable of mixing labeled RNA molecules[12] for ensemble fluorescence measurements.

We used a microfluidic formulator to perform large-scale, automated single-molecule measurements across a wide range of chemical conditions (Fig. 1). The critical fluidic element was a microfluidic mixing ring in which a peristaltic pump made of three integrated valves was used to inject reagents of interest into a ring and in which a second pump circulated and mixed the reagents (Fig. 1a). The dual-layer polydimethylsiloxane (PDMS) device consists of a control layer that uses 'push-down' valves to manipulate fluid on the flow layer, with nominal channel width of 100 μm and height of 10 μm. We detected the molecules of interest in the flow layer using confocal microscopy. Using the first peristaltic pump (Fig. 1a) we injected the contents of seven independently addressable input channels (Supplementary Fig. 1a) into the mixing ring with precision to tens of picoliters. As reagents are pumped into the ring, the reagent valve, inlet valve and outlet valve are opened and previous contents of the ring are displaced. Calculations of final concentrations must take this volume displacement into account.

The push-down valve configuration permits sample detection directly above the glass coverslip, a benefit for single-molecule spectroscopy. An observation chamber (50 μm tall by 250 μm wide) is situated in the mixing ring to allow optimal confocal detection. The ring is then flushed and prepped for a sequential measurement. We developed software for coordination between microfluidic device control and microscopic data acquisition to enable long-term unassisted data collection with high reproducibility (Supplementary Figs. 2–4).

With this device we could automatically perform reagent titrations to screen multidimensional chemical space for conformational and enzymatic changes in biomolecules. The approach allowed for large sampling of parameter space that could not be easily achieved using ensemble-based methods; whereas the single- molecule assay resolves subpopulations (ssDNA, dsDNA and others), an ensemble measurement 'smears' this information into a single, averaged number. We first used an ssDNA probe consisting of a poly(dT) sequence of 20 nucleotides, flanked by donor (5(6)-carboxytetramethylrhodamine) and acceptor (Alexa Fluor 647) dyes at the 3′ and 5′ ends of the nucleotide backbone (called poly(dT) hereafter). We used smFRET as a readout to resolve changes in DNA polymer conformation resulting from compaction and hybridization.

We first sampled the poly(dT) conformation as a function of ionic strength in the microfluidic device. We performed consecutive smFRET measurements of poly(dT) in automatically titrated salt concentrations. We plotted each measurement as a scatter plot with dimensions of FRET, approximated by the 'proximity ratio', and of dye stoichiometry, measured using alternating laser excitation spectroscopy[13]. In each two-dimensional plot, each point represents a single molecule; donor-acceptor molecules of interest are found in the center half of the stoichiometry axis (stoichiometry of 0.25 to 0.75) (Fig. 1b). As expected, ssDNA molecules collapsed (lower end-to-end distance, higher FRET) upon ionic strength increase owing to ionic screening and consequent reduction in persistence length (Fig. 1d and Supplementary Fig. 5a). We also studied DNA conformation with five different cations, in which the magnitude of each salt effect followed the order of Hofmeister series (Supplementary Fig. 5b).

This approach allowed us to study the ssDNA conformation and hybridization efficiency (to a complementary strand) under the influence of two competing processes: increase in rigidity resulting from hybridization and chain collapse resulting from an increase in ionic strength. We conducted 64 serial measurements comprised of an eight-increment NaCl concentration gradient and an eight-increment complementary strand concentration gradient (Fig. 1) to analyze the differential effects of hybridization (causing lower FRET) and ionic strength (causing higher FRET) on ssDNA. We observed coexistence of ssDNA and dsDNA sub-populations in some cases (Fig. 1d). We fit subpopulations to two-dimensional Gaussian distributions and extrapolated concentrations from the volume under each subpopulation's fit; we represented the extent of hybridization as the ratio, R = [dsDNA] / ([dsDNA] + [ssDNA]). At the lowest salt and complementary strand concentrations, hybridization efficiencies were negligibly low (Fig. 1c), and we observed chain collapse caused by increasing ion content. At complementary strand concentrations greater than 7 nM, the hybridizing effect (low FRET population) dominated the chain collapse effect (high FRET population) as cation concentration increased. Thus, increase in ionic strength not only promoted ssDNA compaction but also promoted hybridization.

Theoretical estimates for the poly(dT) hybridization midpoint were in agreement with the midpoints we observed (Supplementary Fig. 6). We therefore recapitulated a large two-dimensional titration to directly measure the hybridization landscape of ssDNA to its complement in 64 different chemical environments. Screening a large phase-space of physicochemical parameters is crucial, for example, for the design of biologically relevant aptamers, molecular beacons or short interfering RNA constructs. To assess the higher dimensionality accessible with this technique, we titrated two salts, NaCl and $MgCl_2$, against poly(dA). The resulting three-dimensional hybridization phase map (Supplementary Fig. 7) revealed the comparative and combinatorial effects of the monovalent and divalent salts on ssDNA compaction and hybridization.

We extended this approach to the study of enzyme activity, exploiting the poly(dT) probe as a biosensor for productive mRNA synthesis by bacterial RNA polymerase (RNAP). Previous reports have established dependence of RNAP activity on glutamate concentration, showing that the osmolyte acts as both a positive and negative regulator of transcription, depending on the absolute glutamate concentration[14]. Glutamate facilitates RNAP promoter escape, enabling productive transcription, by altering the RNAP conformation (likely owing to the Hofmeister effect). Conversely, high concentrations of glutamate are reported to cause considerable decreases in transcription by inhibiting RNAP from binding to the ribosomal promoters. Our optofluidic single-molecule transcription assay allowed thorough exploration of the glutamate response space for RNAP activity.

We designed a DNA template for transcription such that the RNA transcript would hybridize to poly(dT) (Fig. 2a). Maintaining a constant poly(dT) concentration (250 pM), we titrated RNAP in six increments and potassium glutamate in six increments (Fig. 2b). Here low-FRET species correspond to DNA-RNA heteroduplexes of poly(dT) hybridized to the mRNA transcripts. The volume under the low-FRET peak therefore scaled with productive mRNA synthesis (Fig. 2b). Fitting each subpopulation to obtain a hybridization ratio provides a metric to directly quantify RNA transcripts.

Although changes to glutamate concentration affect ssDNA conformation, hybridized and unhybridized subpopulations were clearly resolved. Increases in hybridized transcript were apparent with increasing RNAP and glutamate concentrations until excessive concentrations of glutamate (514 mM) were reached (Fig. 2), consistent with previous observations of glutamate inhibition at concentrations >500 mM[14]. Although the contribution of ionic

strength to hybridization efficiency could, in principle, complicate this readout, this effect appears to be minimal when measured directly (Supplementary Fig. 8).

In contrast to traditional approaches to transcript detection, the single-molecule approach can be used to detect very low concentrations of RNA; for instance at 50% hybridization, we expected only ~100 pM RNA transcript in only a few nanoliters. Using this approach, we sampled enzyme activity in a large physiochemical space. The possibilities for this type of multiparameter inquiry may help to understand the complex and multifactorial mechanisms underlying transcriptional regulation and other similarly complex enzymatic systems.

The ability to observe multiparameter physiochemical landscapes without having to manually dilute and load the sample on the microscope substantially simplifies the process and dramatically reduces variability during titration. Whereas typical pipetting error can be around 0.5%, or 50 nl for microliter reactions, the ring injection error is ~0.0001%[11]. A possible enhancement to the approach presented here would take advantage of emerging multispot photon-counting detectors[15].

The high-throughput analysis of conformational landscapes may considerably enrich studies of protein regulation, interaction networks, allostery and folding. Moreover, in its ability to quantify small amounts of mRNA, this technique represents meaningful progress toward single-cell gene expression profiling.

METHODS

Methods and any associated references are available in the online version of the paper at http://www.nature.com/naturemethods/.

Supplementary Material

Refer to Web version on PubMed Central for supplementary material.

Acknowledgments

We thank R. Colyer, P. Blainey and other members of the Weiss and Quake laboratories for helpful discussions. This work was supported by US National Science Foundation Frontiers in Integrative Biological Research grant 0623664 and National Institutes of Health grant GM069709. Fluorescence spectroscopy was performed at the University of California, Los Angeles and California NanoSystems Institute Advanced Light Microscopy and Spectroscopy Shared Facility. A.M.S. was supported by the Stanford University Diversifying Academia, Recruiting Excellence fellowship.

ONLINE METHODS

DNA

All oligonucleotides were synthesized and purified by high-performance liquid chromatography (IDT Technologies) (Supplementary Table 1).

Buffers

All measurements (except those for RNAP) were conducted in 10 mM Tris (pH 8.0) and 50 mM NaCl. RNAP assays were conducted in 40 mM HEPES, 10 mM $MgCl_2$, 1 mM DTT, 100 μg ml^{-1} BSA, 5% glycerol and 1 mM β-mercaptoethylamine (pH 7.0) containing 2.8 mM NTP mixture.

RNAP assays

We incubated 1.6 μl of commercially purified 1.111 μM RNAP holoenzyme (Epicentre) with 0.6 μl of 1 μM template DNA at 37 °C in 26 μl of 50 mM Tris HCl, 100 mM KCl, 10 mM $MgCl_2$, 1 mM DTT, 100 μg ml^{-1} BSA and 5% glycerol (pH 8.0) for 15 min to form the RNAP open complex (RP_O). This mixture was challenged with heparin sepharose resin as described previously[16] to eliminate nonspecific complexes. The RP_O solution was diluted to a final concentration of 2 nM and loaded on the sample channel of the PDMS chip. Assays were performed at room temperature (19 °C) as productive transcription occurs well below the optimal 37 °C. Samples were incubated in the mixing ring for 15 min before measurement to facilitate transcription. As anticipated, negligible transcript was detected in the absence of RNAP; this was also the case in the presence of RNAP inhibitors or in the absence of DNA template or proper nucleotides (data not shown). RNAP stability was measured over the timescale of several hours and shown to yield identical results within experimental error (s.d. = 0.04) (Supplementary Fig. 4).

Microfluidic device fabrication

Standard soft lithography techniques were used to fabricate microfluidic devices with integrated valves and pumps[17]. The coverslip (number 1, ~0.15-μm thickness) and PDMS cast were irradiated for 30 s in a plasma chamber and subsequently placed upon one another and kept at 80 °C for 10 min. Instructions and parts for building the micro-fluidics setup and the valve controller software are available at http://www.stanford.edu/group/foundry/. Software for hardware control and acquisition is available as Supplementary Software and Supplementary Note and at http://sourceforge.net/projects/uformulator/files/.

Microfluidic device characterization and calibration

For each channel, peristaltic pump injections were calibrated using fluorescence readouts (Alexa Fluor 488, free dye). The precise amount of injected volume per slug or injection cycle was determined by measured fluorescence intensity in the mixing ring from a single slug normalized to the intensity of 100% Alexa Fluor 488 solution in the mixing ring. For all channels, a single injection slug was 0.4% of the mixing ring volume or a 243-fold dilution of the contents of the ring; calibration curves were generated for device characterization (Supplementary Fig. 2). The relatively high observation chamber in the mixing ring creates a slightly thicker flow layer; to compensate, pressure of the control layer was maintained at 40 pounds per square inch (psi) to ensure complete valve closing. Flow pressure was maintained at 10 psi. To ensure proper mixing, the transient response, as reported by fluorescence intensity, was measured at a fixed point in the ring. The time to establish steady-state mixing was characterized and used in all subsequent measurements (Supplementary Fig. 9). Reproducibility of measurement was assessed by conducting a 4 × 4 hybridization-by-salt measurement, performing the serial titrations in both the forward and reverse sequence, which yielded identical results, as indicated by the heatmaps of respective hybridization (Supplementary Fig. 3). To prevent cross-contamination and sample loss from surface adsorption, flow channels were incubated with 0.5% of Pluronic F-127 for 1 h.

Estimation of DNA hybridization midpoints

The melting temperature (T_M) at 1 M NaCl was estimated from the nearest-neighbor two-state model[18]:

$$T_{\mathrm{M}}\,(^{\circ}\mathrm{C}) = \frac{\Delta H^{\circ}}{\Delta S^{\circ} - R \ln[\mathrm{oligo}]} - 273.15$$

with R, the ideal gas constant (1.987 cal K^{-1} mol^{-1}), and the thermodynamic parameters of formation (enthalpy, $\Delta H°$, and entropy, $\Delta S°$) reported in reference [19].

The theoretical monovalent ion concentration, $[Na^+]$, at 50% hybridized form at fixed oligonucleotide concentration, [oligo], was extrapolated from the following equation reported in reference [20]:

$$\frac{1}{T_{\mathrm{M}}\,(\mathrm{Na}^+)} = \frac{1}{T_{\mathrm{M}}\,(1\quad \mathrm{M}\quad \mathrm{Na}^+)} + \left((4.29\quad f_{\mathrm{GC}} - 3.95)\ln[\mathrm{Na}^+] + 0.940\ln^2[\mathrm{Na}^+]\right)\times 10^{-5}$$

in which f_{GC} is the fraction of the G+C content in the oligo (in our case, 0).

RNA quantification

The free energy of hybridization of 20-base-pair dsDNA is large enough (about –18 kcal mol^{-1} at 1 M NaCl) that, as experimental measurements show, essentially all single strands hybridize at a 1:1 ratio of $d(A)_{20}$ to $d(T)_{20}$ (Supplementary Fig. 10). An RNA-DNA heteroduplex is known to have similar free energy of hybridization (~–16 kcal mol^{-1} at 1 M NaCl)[21], and so we consider it reasonable to assume complete hybridization and quantify mRNA transcripts by multiplying the measured R by the amount of probes in each experiment (250 pM). Furthermore, we can conclude that our assay is a single-round, run-off transcription assay because the area under the dsDNA population curve did not change with increasing incubation time (data not shown). Other studies have reported the timescale for complete hybridization of 20 base pairs to be considerably shorter than our experimental timescales[22]. Because an RNAP complex can only produce a single mRNA, we can relate the amount of mRNA transcripts to promoter clearance of RNAP. For instance, at 569 pM RNAP and 143 mM glutamate with 250 pM probes (Fig. 2a), R = 0.75. This corresponds to 187.5 pM mRNA or 33% ‘active’ RNAP complexes in this condition.

Single-molecule spectroscopy

Single-molecule measurements were performed as described previously23 with slight alterations to microscope setup construction. Briefly, a home-built confocal microscope setup based around an Olympus IX-71 body was used in this study with Plan-Apo 1.4 numerical aperture (NA) 63× oil-immersion objective (Zeiss). Alternating excitation of fluorophores was accomplished using acousto-optic modulator (NEOS Technologies) and continuous-wave 532 nm (CNI) and 635 nm (Coherent) lasers. Confocal detection through a 100 μm pinhole used avalanche photodiodes (Perkin Elmer); a 635 DCXR dichroic mirror (Chroma) and two filters (580 DF60 for donor and 665LP for acceptor (Chroma)) were used to spectrally separate emitted photons. The observation chamber (50 μm) permitted focusing the objective lens 20 μm into the sample preventing stray light from scattering off the coverslip or channel walls. The larger observation chamber also allowed the point spread function of the oil-immersion objective to fit in the flow channel. To avoid evaporation of the medium between the coverslip and the objective during our long experiments, an oil objective was preferred over a water objective. These data collection parameters yielded detection of single-molecule bursts identical to those collected under similar conditions in the absence of any microfluidic device. Data were collected for 20 min per measurement; a

LabView routine was written to permit communication between spectroscopic data acquisition software and the microfluidic controller apparatus for full automation. Each molecule was detected as a 'burst' of fluorescence, from which two ratiometric values were extracted: FRET (reporting on distance between dyes) and stoichiometry ('S', reporting on whether the molecule contains both donor and acceptor (S = 0.5) or donor only or acceptor only (S = 1, S = 0, respectively). FRET and stoichiometry determination was performed as described previously[23]; but, as this study was not concerned with precise determination of distances but ratio of subpopulations, the FRET measurement was defined simply as the 'proximity ratio' ((acceptor photons)/(all emitted photons) during donor excitation).

References

1. Maxwell KL, et al. Protein Sci. 2005; 14:602–616. [PubMed: 15689503]
2. Ha T, et al. Proc. Natl. Acad. Sci. USA. 1996; 93:6264–6268. [PubMed: 8692803]
3. Melin J, Quake SR. Annu. Rev. Biophys. Biomol. Struct. 2007; 36:213–231. [PubMed: 17269901]
4. Squires TM, Quake SR. Rev. Mod. Phys. 2005; 77:977–1026.
5. Hamadani KM, Weiss S. Biophys. J. 2008; 95:352–365. [PubMed: 18339751]
6. Hertzog DE, et al. Anal. Chem. 2004; 76:7169–7178. [PubMed: 15595857]
7. Lipman EA, Schuler B, Bakajin O, Eaton WA. Science. 2003; 301:1233–1235. [PubMed: 12947198]
8. Pfeil SH, Wickersham CE, Hoffmann A, Lipman EA. Rev. Sci. Instrum. 2009; 80:055105. [PubMed: 19485532]
9. Vandelinder V, Ferreon AC, Gambin Y, Deniz AA, Groisman A. Anal. Chem. 2009; 81:6929–6935. [PubMed: 19555081]
10. Lemke EA, et al. J. Am. Chem. Soc. 2009; 131:13610–13612. [PubMed: 19772358]
11. Hansen CL, Sommer MO, Quake SR. Proc. Natl. Acad. Sci. USA. 2004; 101:14431–14436. [PubMed: 15452343]
12. Ridgeway WK, Seitaridou E, Phillips R, Williamson JR. Nucleic Acids Res. 2009; 37:e142. [PubMed: 19759214]
13. Kapanidis AN, et al. Proc. Natl. Acad. Sci. USA. 2004; 101:8936–8941. [PubMed: 15175430]
14. Gralla JD, Huo YX. Biochemistry. 2008; 47:13189–13196. [PubMed: 19053283]
15. Colyer RA, et al. Proc. SPIE. 2010; 7571:75710G.
16. Kapanidis AN, et al. Science. 2006; 314:1144–1147. [PubMed: 17110578]
17. Unger MA, Chou H-P, Thorsen T, Scherer A, Quake SR. Science. 2000; 288:113–116. [PubMed: 10753110]
18. Zimm BH, Roe GM, Epstein LF. J. Chem. Phys. 1956; 24:279–280.
19. Allawi HT, SantaLucia J. Biochemistry. 1997; 36:10581–10594. [PubMed: 9265640]
20. Owczarzy R, et al. Biochemistry. 2004; 43:3537–3554. [PubMed: 15035624]
21. Sugimoto N, et al. Biochemistry. 1995; 34:11211–11216. [PubMed: 7545436]
22. Erickson D, Li D, Krull UJ. Anal. Biochem. 2003; 317:186–200. [PubMed: 12758257]
23. Majumdar DS, et al. Proc. Natl. Acad. Sci. USA. 2007; 104:12640–12645. [PubMed: 17502603]

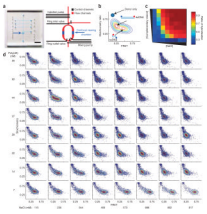

Figure 1.

A microfluidic formulator for high-throughput single-molecule FRET measurements. (**a**) Device image (left) with the mixing ring highlighted (arrow). Scale bar, 5 mm. The schematic (right) depicts critical features of the control and flow layer (control and flow channels). (**b**) A schematic plot representing smFRET measurements as a two-dimensional histogram of FRET versus stoichiometry. The subpopulations of interest are hybridized poly(dT) (low FRET population; dsDNA) and unhybridized poly(dT) (high FRET population; ssDNA). (**c**) Heat map of hybridization efficiency (ratio of dsDNA to total DNA) for various concentrations of NaCl and complementary strand. (**d**) Matrix of FRET-stoichiometry scatter plots with contour overlay of fits used to generate heat map shown in **c**.

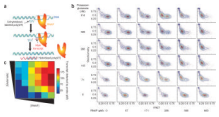

Figure 2.

RNAP activity measured with smFRET. (**a**) A schematic of the assay depicts RNAP transcribing the template, thus producing complementary transcript that hybridizes to the poly(dT) probe. (**b**) A matrix of FRET-stoichiometry scatter plots (as in fig. 1) depicting hybridization of the poly(dT) probe to newly produced transcript upon titrating RNAP and glutamate. (**c**) Heat map showing quantification of the data in **b**. Amount of transcript is plotted for various concentrations of RNAP and glutamate.